HHS Public Access

Author manuscript

Neuron. Author manuscript; available in PMC 2019 December 05.

Published in final edited form as:

Neuron. 2018 December 05; 100(5): 1059–1065.e4. doi:10.1016/j.neuron.2018.10.011.

Light prior to eye-opening promotes retinal waves and eye-specific segregation

Alexandre Tiriac[1], **Benjamin E. Smith**[2], and **Marla B. Feller**[1,3]

[1]Department of Molecular and Cell Biology, University of California, Berkeley, Berkeley, CA 94720, USA

[2]School of Optometry, University of California, Berkeley, Berkeley, CA 94720, USA

[3]Helen Wills Neuroscience Institute, University of California, Berkeley, Berkeley, CA, 94720, USA

Abstract

Retinal waves are bursts of correlated activity that occur prior to eye-opening and provide a critical source of activity that drives the refinement of retinofugal projections. Retinal waves are thought to be initiated spontaneously with their spatiotemporal features dictated by immature neural circuits. Here we demonstrate that, during the second postnatal week in mice, changes in light intensity dictate where and when a subset of retinal waves are triggered via activation of conventional photoreceptors. Propagation properties of triggered waves are indistinguishable from spontaneous waves, indicating that they are activating the same retinal circuits. Using whole brain imaging techniques, we demonstrate that light deprivation prior to eye-opening diminishes eye-specific segregation of the retinal projections to lateral geniculate nucleus of the thalamus but not other retinal targets. These data indicate that light that passes through the closed eyelids plays a critical role in the development of the image-forming visual system.

eTOC Blurb:

Tiriac, Smith and Feller show that prior to eye-opening, glutamatergic waves can be triggered with light with spatiotemporal precision. They show that dark rearing prior to eye-opening reduces eye-specific segregation of retinal afferents to the dorsal lateral geniculate nucleus.

Lead Contact: MBF (mfeller@berkeley.edu).

Author Contributions

Conceptualization, A.T., B.E.S, and M.B.F.; Methodology, A.T., B.E.S, and M.B.F.; Software, A.T. and B.E.S; Formal Analysis, A.T., B.E.S, and M.B.F.; Investigation, A.T.; Writing – Original Draft, A.T., B.E.S, and M.B.F.; Writing – Review & Editing, A.T., B.E.S, and M.B.F.; Visualization, A.T., B.E.S, and M.B.F.; Funding Acquisition, M.B.F.

Competing Interests statement

The authors declare no competing financial interests.

DATA AND SOFTWARE AVAILABILITY

Detection of retinal waves software. https://github.com/Llamero/Retinal_Wave_Vector_Flow-Macro.

The datasets generated during and/or analyzed during the current study and all custom scripts and functions generated or used during the current study are available from the Lead Contact (mfeller@berkeley.edu) on request.

Graphical Abstract

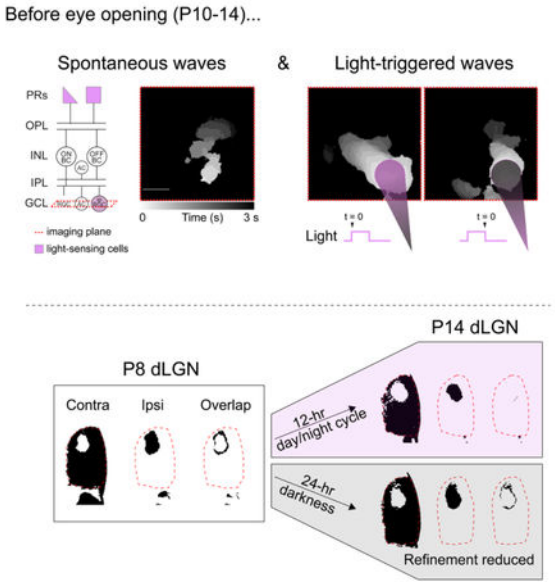

INTRODUCTION

Retinal waves are highly correlated spontaneous firing patterns that propagate throughout the developing retina (Blankenship and Feller, 2010; Kerschensteiner, 2016). In mice, retinal waves are first detected a few days before birth and persist for approximately two weeks after birth, disappearing around the time of eye-opening. During this developmental period, the retinal circuits mediating waves also change. At postnatal day 1 (P1), waves are mediated by a transient cholinergic circuit in which recurrent excitatory connections between starburst amacrine cells initiate and propagate retinal waves. At P8–10, bipolar cell synapses mature and waves become dependent on activation of ionotropic glutamate receptors .

Retinal waves propagate beyond the retina to the superior colliculus, thalamus, and primary visual cortex (Ackman et al., 2012; Murata and Colonnese, 2016) and play an important role in the segregation of retinogeniculate axons and the formation of retinotopic maps before eye-opening (for recent reviews, see Assali et al., 2014; Huberman et al., 2008; Kirkby et al., 2013; and Thompson et al., 2017). For example, in mice, contralateral and ipsilateral retinal projections to the dorsal lateral geniculate nucleus (dLGN) of the thalamus initially overlap at P3, segregate into eye-specific regions that are apparent by P8, and continue to segregate until eye-opening at P14. Significant alterations of retinal waves at any of these time points significantly reduce this segregation.

In addition to retinal waves, evoked light responses are also present throughout development. During cholinergic retinal waves, intrinsically photosensitive retinal ganglion cells (ipRGCs) are present, respond to light, and influence retinal circuits via axon collaterals and/or gap junction coupling (Arroyo et al., 2016; Kirkby and Feller, 2013; Renna et al., 2011). These early light responses contribute to photoentrainment of circadian rhythms (Duncan et al.,

1986), light avoidance (Johnson et al., 2010), vascularization of the eye (Rao et al., 2013), and the maturation of synapses within the retina (Dunn et al., 2013).

At the same age that glutamatergic waves appear, the earliest rod- and cone-mediated light responses are observed in retinal ganglion cells (RGCs) (Tian and Copenhagen, 2003) (Figure 1a). These earliest light-responsive cells already exhibit many functional properties including categorization into ON, OFF, and ON-OFF cells (Tian and Copenhagen, 2003) as well as direction selectivity (Chen et al., 2009; Rosa et al., 2016). Moreover, visual stimulation through the closed eyelids of developing ferrets drive responses in LGN and V1, with structure of the visual scene encoded by immature receptive fields in both of these brain structures (Akerman et al., 2002, 2004).

Here we investigate how structured light contributes to glutamatergic retinal waves and whether light influences the eye-specific refinement of retinal projections to image-forming centers in the brain prior to eye-opening.

RESULTS

Light modulates the frequency of glutamatergic waves.

To characterize the influence of light stimulation on waves, we conducted two-photon calcium imaging experiments on retinas expressing GCaMP6f under the synapsin-1 promoter, which labels all retinal neurons in the ganglion cell layer (Borghuis et al., 2011; Zariwala et al., 2012) (Figure S2c). Two age ranges were used - P6-P8 to isolate cholinergic waves and P11-P13 to isolate glutamatergic waves. All retinas exhibited spontaneous wave activity (Figure 1a-c and Figure S1a-c). To stimulate the retina, we used a light intensity equal to or less than the calculated amount of sunlight that passes through the eyelids of a P12 mouse (Johnson et al., 2010). We found that isolated eyelids from mouse pups transmitted 20% of 375 nm light and exhibited 28% spatial frequency modulation and retained 28% contrast for structures 330 μm in diameter (Supplemental Figure S2).

In P6-P8 retina, stimulation with 375 nm light spots did not initiate waves. In contrast, in P11-P13 retina, light spots initiated waves roughly 50% of the time. These triggered waves initiated at the location of the light stimulus, propagated beyond the boundaries of the light stimulus, and initiated precisely at the dark-to-light (ON-initiated waves) and light-to-dark transitions (OFF-initiated waves) (Figure 1d and Movie S1).

To quantify the impact of visual stimulation on retinal wave initiation, we compared several scenarios: constant dark, constant light, and pulsed light, for which the frequency of waves was assessed outside the region where the retina was directly stimulated. Cholinergic retinal waves initiated at a rate of 1.26 ± 0.21 waves/minute, and this frequency was not impacted by any of the light conditions (Figure S1 d-f), consistent with previous studies (Kirkby and Feller, 2013; Renna et al., 2011). Glutamatergic waves initiated at a rate of 1.02 ± 0.14 waves/minute and 0.52 ± 0.081 waves/minute in constant dark or constant light, respectively. In contrast to cholinergic waves, glutamatergic wave initiation was greatly increased by light pulses occurring 2–3 times/minute (2.48 ± 0.19 waves/minute; Figure 1e-f). Glutamatergic waves initiated by light occurred following the change in luminance (Figure 1g). These data

are consistent with the frequency of waves being determined by a combination of spontaneous waves (waves that were not time-locked to a light stimulus) and light-triggered glutamatergic waves.

Blocking photoreceptor to bipolar cell signaling abolishes light-evoked wave initiation.

To determine if light-evoked waves were initiated by activation of conventional photoreceptors or ipRGCs, we compared the success rate of triggering a wave with a light pulse in the absence and presence of drugs that block photoreceptor-bipolar cell synapses. In the absence of drugs, ON-initiated waves had a success rate of 45% ± 0.51% (n = 3 retinas, 160 light stimuli total) and OFF-initiated waves had a success rate of 40% ± 4.3% (n = 3 retinas, 160 light stimuli) (Figure 2). Application of the mGluR6 agonist L-AP4 (20 μM), which blocks photoreceptor to ON-bipolar cell signaling (Slaughter and Miller, 1981), blocked ON-initiated waves and increased the success rate of OFF-initiated waves (86 ± 13%). Application of UBP 310 (50 μM), which blocks photoreceptor to OFF bipolar cell signaling (Borghuis et al., 2014; Puthussery et al., 2014) in isolation blocked OFF-initiated waves (Figure 2b, bottom). Application of both UBP 310 and L-AP4 completely blocked both ON- and OFF-initiated waves (Figure 2b). Note that ipRGC light responses were retained in the presence of L-AP4 and UBP 310 (Figure 2a, top). Together, these results strongly indicate that light-evoked waves are initiated by cone and rod photoreceptor signaling and not ipRGCs.

Light-triggered and spontaneous waves have similar spatiotemporal properties and recruit the same retinal circuits.

To test whether light-triggered glutamatergic waves activated the same retinal circuits as spontaneous waves, we compared several wave features. First, we found no difference in propagation speed or total propagation area between spontaneous and light-evoked waves (Figure 3a). Second, we compared the proportion of ON, ON-OFF, OFF, and non-light-responsive (NR) cells in the ganglion cell layer (Figure 3b middle and 3c left) that participated in spontaneous and light-evoked waves (see Supplemental methods for discussion of this categorization). Both the spontaneous and light-evoked waves, waves could be clustered into distinct groups (Figure 3c): in one group, waves recruited most ON cells and about half of the ON-OFF cells. In the second group, waves recruited most OFF, ON-OFF, and NR cells but very few ON cells. Finally, we quantified how similarly individual cells participated in light-triggered and spontaneous waves using an Unweighted Pair Group Method with Arithmetic Mean (UPGMA) hierarchy and did not find a significant difference between these waves (Figure 3c, right). Hence, we conclude that light-evoked and spontaneous retinal waves activate the same microcircuits and that light stimulation influences primarily the initiation rate of glutamatergic waves.

Mice reared in darkness before eye-opening exhibit reduced eye-specific segregation.

To determine the impact of light on the development of the visual system before eye-opening, we assessed the effects of dark rearing on eye-specific segregation of retinal ganglion cell projections to the dorsal lateral geniculate nucleus (Figure 4a). Examining eye-specific segregation of fluorescently labelled anterograde tracers is a canonical approach used to identify mechanisms that influence this activity-dependent developmental process

[for review, see (Huberman et al., 2008)]. We used brain clearing techniques and whole brain imaging for volumetric assessment of eye-specific segregation within the dLGN as well as other retino-recipient regions that receive binocular projections (Figure 4b and Movies S2-3). We used a threshold-independent approach to quantify the amount of segregation. This approach, modified from (Torborg and Feller, 2004), is based on computing the log ratio of fluorescence intensity from the ipsilateral-projecting axons over the fluorescence intensity of the contralateral-projecting axons for each voxel in a region of interest. We focused our analysis on the anterior third of the dLGN (~70 coronal optical slices each 6.15 μm thick, total thickness ~430 μm) where the ipsilateral and contralateral retinogeniculate projections are most segregated (Figure 4c-d).

Dark rearing from birth or from P8–P14 largely prevented the eye-specific refinement that normally occurs from P8 to P14 (Figures 4C–4E). Combined with our ex vivo results, these findings are consistent with the hypothesis. Our ex vivo experiments suggest that dark rearing reduces glutamatergic wave frequency; we thus hypothesized that dark rearing specifically from P8 to P14 would prevent the development of eye-specific segregation. Returning mice to a regular light cycle after dark rearing for the first 2 weeks of postnatal life did not rescue eye-specific segregation deficits by P30 (Figure 4Figures 4F and S3D).

We compared our findings that dark-rearing reduced eye-specific refinement in the dLGN to other binocular regions, including the ventral lateral geniculate nucleus (vLGN) and the olivary pretectal nucleus (OPN) (Figure S3). In contrast to our findings in the dLGN, dark rearing had no impact on the other retinorecipient regions, specifically the vLGN and the OPN. (Note, we also investigated the SC but found that our analysis methods could not detect any overlap between ipsi and contra projections at P8 and therefore excluded the SC from this analysis). Thus, visual experience prior to eye opening influences the activity-dependent refinement of retinal projections to the visual thalamus.

DISCUSSION

Here we demonstrate for the first time that visual stimuli through the closed eyelids instruct when and where glutamatergic retinal waves initiate, and that this instruction plays a role in the eye-specific refinement of retinogeniculate projections. We also showed that light induced initiation of waves is mediated by cone and rod signaling to bipolar cells, and not by ipRGCs, and that changes in luminance do not affect wave frequency during the first postnatal week when cholinergic waves occur. Evoked and spontaneous glutamatergic waves have the same propagation speed, propagation area, and appear to activate the same microcircuits within the retina. Lastly, we showed that retinal projections to various targets in the brain undergo eye-specific segregation from P8 to P14, but that visual experience prior to eye-opening specifically affects retinal projections to the dLGN. Finally, we showed that dark-rearing before eye-opening leads to persistent deficits in eye-specific segregation. These findings implicate a previously unknown role of visual experience prior to eye-opening in directing the refinement and maturation of visual circuits.

Implications for wave generating circuits

We found that light altered the frequency of glutamatergic but not cholinergic retinal waves. This finding is consistent with previous reports that showed that light stimulation of ipRGCs impacts the duration of action potential bursts during cholinergic waves but not the rate of spontaneous initiation (Kirkby and Feller, 2013; Renna et al., 2011). Rather, cholinergic retinal waves are initiated by the spontaneous depolarizations of cholinergic interneurons, called starburst amacrine cells. The frequency of cholinergic waves is influenced by a refractory period mediated by slow afterhyperpolarization in starburst amacrine cells (Ford et al., 2012; Zheng et al., 2006).

In contrast, the circuit mechanisms that determine the frequency of glutamatergic waves are less understood. Glutamatergic waves are thought to be initiated by stochastic depolarizations of bipolar cells and propagate laterally via excitatory volumetric glutamatergic transmission and electrical synapses (Kerschensteiner, 2016). Our results indicate that the initiation of glutamatergic waves is controlled at least in part by photoreceptor to bipolar cell signaling. Further experiments will be needed to determine whether this synapse is also the source of initiation of spontaneous glutamatergic waves in the absence of light.

Comparisons with previous studies of eye-specific segregation

We observed a reduction in eye-specific segregation induced by dark-rearing prior to eye-opening (Figure 4). The magnitude of this reduction is comparable to several other manipulations that disrupt eye-specific segregation (Kirkby et al., 2013), including interference with the complement cascade [for example, see (Bialas and Stevens, 2013)], targeted killing of ipRGCs (Chew et al., 2017), and disruption of glutamatergic waves (Blankenship et al., 2011; Hamby et al., 2015; Xu et al., 2010). Interestingly, we found that retinal projections to non-image-forming parts of the brain—the vLGN and OPN—undergo developmental eye-specific refinement, but not in a light-dependent manner (Figure S3). This is consistent with the idea that early visual activity may be critical specifically for early organization of circuits that mediate vision.

However, our results contradict previous findings on the role of light before eye-opening. One study observed no difference in eye-specific segregation in the dLGN between dark-reared and light-reared (12 hr day/night cycle) mice (Demas et al., 2006). We hypothesize that the difference is likely to be a variation in the amount of segregation observed in different sections of the dLGN (see Figure S4); this variation is minimized by using volumetric analysis, which was not possible in the previous studies based on epifluorescence imaging of dLGN sections. Similarly, dark-rearing prior to eye-opening did not impact synaptic pruning of retinogeniculate projections (Hooks and Chen, 2006), a process that was not assessed here. However, this same study did conclude that visual experience prior to and around eye-opening was important for allowing activity-dependent retinotopic refinement that occurs later in development, indicating early visual experience impacts retinogeniculate synapses or circuits.

It was also reported that retinogeniculate axons segregate normally in a $Crx^{-/-}$ mouse, in which photoreceptors fail to make connections with bipolar cells and thereby have no rod and cone-mediated light responses (Soto et al., 2012), in seeming contradiction with our results. However, Soto et al. showed that, in the absence of cone and rod photoreceptor input, there is enhanced correlated neural activity in retinal ganglion cells specifically when glutamatergic waves are present. This increase in RGC neural activity in the $Crx^{-/-}$ mice is therefore not a good model for comparing to dark-rearing, which exhibits a decrease in glutamatergic wave frequency.

Do ipRGCs play a role in eye-specific segregation? Mice that lack melanopsin have less eye-specific segregation of retinogeniculate afferents than control mice raised in 24 hours of continuous light (Renna et al., 2011) but similar eye-specific segregation when mice are raised in normal lighting conditions (Chew et al., 2017). These studies strongly suggest that ipRGC-mediated light responses do not play a role in the development of eye-specific segregation. However, targeted killing of a subpopulation of ipRGCs does reduce eye-specific segregation (Chew et al., 2017). Hence, ipRGCs may be critical for eye-specific segregation via their role in wave-propagating circuits rather than via their light responses.

Implications for activity-dependent refinement of retinofugal projections

Natural scenes aren't random, but rather have innate statistical structure. Given our findings that light-triggered glutamatergic waves are space- (Figure 1d) and time-locked (Figure 1g) to light stimuli, natural scenes, even through the closed eyelids (Akerman et al., 2004), likely influence the spatiotemporal properties of glutamatergic waves. As a result, the visual system during the period when glutamatergic waves occur may develop in a way that ideally suits the statistical structure of the visual environment. Indeed, recent findings have revealed a rich complexity of retinal projections to the dLGN, with individual thalamic neurons receiving inputs from a variety of RGC subtypes (Liang et al., 2018; Morgan et al., 2016; Rompani et al., 2017) and RGCs even of the same subtype exhibiting different projection patterns depending on location in the LGN (Hong et al., 2018). Moreover, many LGN neurons at the boundary between ipsilateral and contralateral RGC projections have functional binocular inputs and the strength of this binocularity is altered via monocular deprivation (Jaepel et al., 2017; Sommeijer et al., 2017). Future experiments will determine the role of spontaneous and evoked activity in the maturation of the precise synaptic inputs of retinogeniculate axons onto thalamic neurons.

STAR Methods

CONTACT FOR REAGENT AND RESOURCE SHARING

Further information and requests for resources and reagents should be directed to and will be fulfilled by the Lead Contact, Marla B. Feller (mfeller@berekeley.edu).

EXPERIMENTAL MODEL AND SUBJECT DETAILS

Animals.—All mice used in this study were younger than 14 days of age and were of both sexes. To image calcium activity in retinal neurons, GCaMP6f;syn1-cre mice were generated by cross breeding the Ai95(RCL-GCaMP6f)-D (Jackson laboratories) transgenic mouse to

the B6.Cg-Tg(Syn1-cre)671Jxm/J (Jackson laboratories) reporter mouse. All animal procedures were approved by the UC Berkeley Institutional Animal Care and Use Committee and conformed to the NIH *Guide for the Care and Use of Laboratory Animals*, the Public Health Service Policy, and the SFN Policy on the Use of Animals in Neuroscience Research. All animals used for the two-photon imaging experiments were housed 12-hour day/night cycle rooms.

For the study on eye-specific segregation, we used wild-type C57BL/6J (Jackson laboratories). The light-reared (LR) mice were born and raised in a 12-hour day/night cycle. P0-P14 dark-reared (DR) mice were born and raised in a room that is dark 24 hours a day. P8-P14 DR mice were born and raised in LR conditions from P0-P8 and then raised in DR conditions from P8-P14. For the P30 experiments, a subset of mice were raised in darkness until P14 and then in a 12-hour day/night cycle. The LR P30 mice were raised in a 12-hour day/night cycle from birth. All animal husbandry is conducted with red light, which minimizes stimulation of photoreceptors.

METHOD DETAILS

Retina preparation.—Mice were deeply anesthetized with isoflurane inhalation and euthanized by decapitation. Eyes were immediately enucleated and retinas were dissected in oxygenated (95% O_2/ 5% CO_2) ACSF (in mM, 119 NaCl, 2.5 KCl, 1.3 $MgCl_2$, 1 K_2HPO_4, 26.2 $NaHCO_3$, 11 D-glucose, and 2.5 $CaCl_2$) at room-temperature under infra-red illumination. Isolated retinas were mounted whole over a 1–2 mm^2 hole in nitrocellulose filter paper (Millipore) with the photoreceptor layer side down, and transferred in a recording chamber of an upright microscope for imaging. The whole-mount retinas were continuously perfused (3 ml/min) with oxygenated ACSF at 32–34^oC for the duration of the experiment. The retina from the other eye was kept in the dark at room temperature in ACSF bubbled with 95% O_2, 5% CO_2 until use (maximum 8 h).

Two-photon calcium imaging.—Two-photon fluorescence measurements were obtained with a modified movable objective microscope (MOM) (Sutter instruments, Novator, CA) and made using an Olympus 60X, 1.00 NA, LUMPlanFLN objective (Olympus America, Melville, NY) for single cell resolution imaging (FOV: 203 × 203 μm) or a Nikon 16X, 0.80 NA, N16XLWD-PF objective (Nikon, Tokyo, Japan) for large FOV (850 × 850 μm) imaging. Two-photon excitation of GCaMP6f was evoked with an ultrafast pulsed laser (Chameleon Ultra II; Coherent, Santa Clara, CA) tuned to 920 nm. The microscope system was controlled by ScanImage software (www.scanimage.org). Scan parameters were [pixels/ line x lines/frame (frame rate in Hz)]: [128 × 128 (3Hz)], at 2 ms/line. This MOM was equipped with a through-the-objective light stimulation and two detection channels for fluorescence imaging.

A previous study reported that a 2-photon laser at appropriate power for imaging (5–10 mW) can induce light responses (Euler et al., 2009). To account for 2-photon-mediated responses, we adapt retinas to the laser with a 5-minute imaging session, a strategy outlined in the original paper.

Interline visual stimulation.—Visual stimuli patterns were created in imageJ and uploaded to a projector that contains an LED (UV: 375 nm) and a digital micromirror device. To decrease the background signal entering the photomultiplier tubes due to UV stimulation of the GCaMP6f, the stimuli was delivered on the flyback of the fast-axis scanning mirror during a unidirectional scan so as to interleave the stimuli with the imaging. The intensity of the UV stimulus was 2×10^6 photons s^{-1} um^{-2}, which corresponds to the calculated intensity of sunlight through the closed eyelids of a P10 mouse [16]. We used several kinds of stimuli: Circular spots of light with (⌀ 100– 200μm), full field (⌀ 1.7 mm) surround-only (⌀ 1.7 mm excluding scan area), and bottom-only (⌀1 7 mm half circle). All stimuli, except for the spot of light, were delivered either constantly or at a pulsing rate of 0.05 Hz. For the spot of light, the stimuli were presented 4–6 times in a 5-minute movie for 10 seconds each. In all cases, the stimuli had a 100% positive contrast (bright on dark background).

Pharmacological blockade of photoreceptor to bipolar cell signaling.—We blocked ON-bipolar cell signaling via application of the mGluR6 agonist L-AP4 (20 μM; Tocris, part 0103). We blocked photoreceptor to OFF-bipolar cell signaling via application of the kainate receptor antagonist, UBP 310 (50 μM; Tocris, part 3621).

RGC participation in retinal waves.—To determine if spontaneous and light-triggered waves recruit the same retinal circuits, we first identified a FOV with ~ 150 RGCs. A light flash was used to identify ON, OFF, ON-OFF, and non-responsive (NR) RGCs by averaging the RGC responses shortly after the light turns on or off. The retina was imaged until more than 40 spontaneous waves were collected. Retinas were then stimulated with light pulses on the surround to induce light-triggered waves until more than 40 waves were collected.

Eye injections.—P7, P13, and P29 LR and DR mice were injected with cholera toxin subunit B (CTB, Thermo Fisher Scientific, Waltham, MA), which in the retina is taken up by RGCs and labels their axon projections to the brain. Each eye was injected with CTB conjugated to a different fluorophore, specifically Alexa 488 and 647. All eye injections were done in the dark using IR illumination.

Brain clearing.—Mice were euthanized 12 hours later by overdose of isoflurane inhalation. Immediately after breathing stopped, mice were transcardially perfused with 5mL of 4°C phosphate buffered saline (PBS) followed by 5 mL of 4°C 4% paraformaldehyde (PFA). Brains were extracted and stored in PFA overnight at 4°C. Brains were then cleared using CUBIC [17]. Briefly, fixed brains were washed 3×2 hours in room-temperature PBS. Brains were then immersed in reagent 1 solution [weight proportions: 25% urea, 25% N,N,N’,N’-tetrakis(2-hydroxypropyl)ethylenediamine, and 15% polyethylene glycol mono-p-isooctylphenyl ether (aka Triton X-100)] at room temperature for 4–6 days, until brains were cleared. Following another 3×2 hour wash in PBS, brains were immersed in reagent 2 solution [weight proportions: 50% sucrose, 25% urea, and 10% 2,2’,2”-nitrilotriethanol] for another 4–6 days until clear again. The refractive index of the home-made reagent 2 was always tested using a Pocket Refractometer (Atago U.S.A., Inc., Bellevue, WA) to ensure it was 1.45 ± 0.01.

Light-sheet imaging.—Cleared brains were imaged using a Zeiss Lightsheet Z.1 (Carl Zeiss AH, Oberkochen, Germany) system housed by the Molecular Imaging Center (MIC) and Zeiss Berkeley BRAIN-MIC at UC Berkeley. Briefly, brains were cut in half at the midsagittal plane and the rostral-most part of the brain (about 2 mm) and cerebellum were sectioned off. The remaining blocked brain was suspended cortex-down in the light-sheet microscope and the flat coronal plane of the rostral brain was positioned toward the objective. The thalamus, OPN, and SC were imaged individually using a Zeiss 5X, 0.16 NA objective (Zeiss, EC Plan-NEOFLUAR) and optical coronal slices were taken with a step-size of 6.15 μm.

QUANTIFICATION AND STATISTICAL ANALYSIS

Image analysis of retinal waves.—Retinal waves were extracted from background using a custom-made FIJI macro that was run in ImageJ v1.51n. Briefly, the movies were: 1) normalized to a temporal median filter of the movie to remove low temporal frequency background modulation such as photobleaching, 2) high-frequency spatial/temporal noise was removed using a 3D median filter, 3) Local high frequency spatial modulation within the wave was suppressed with a 2D mean filter, 4) a dF/dt stack was created by taking the difference between the stack and the same stack phase shifted one slice, and 5) only the positive dF/dt portion was kept to isolate just the leading edge of the wave. The full code can be found at: https://github.com/Llamero/Retinal_Wave_Vector_Flow-Macro. The dF/dt movies were then transferred to MATLAB for further image analysis. First, a grid of 1×1 pixel was assembled over the visible parts of the retina. A threshold of 50% dF/dt was used to binarize activity in an ROI as having a calcium transient of not. Raster plots were then generated by plotting the ROIs on the y-axis versus time on the x-axis. The sum of active ROIs across time was also generated and was used in addition to the custom FIJI macro described above to count waves. Individual waves were defined as a discrete, continuous dF/dt event that was fully interconnected in space and time. To determine how calcium transients correlated to the change in luminance, we obtained waveforms with a window of 6 seconds centered around every change in luminance and computed the average and standard error of all waveforms. We then shuffled the timing of the changes in luminance *in silico* 1000 times to generate an average waveform independent of stimulus timing. Differences in wave frequency between experimental groups were first determined by performing an ANOVA followed by a Tukey HSD post-hoc test.

To determine if a localized spot of light triggered a wave, we first determined the area of the retina that was directly illuminated by measuring the position and area of the stimulation at the image plane using a grid micrometer and camera in the transmitted light position. We then verified this result *in vivo* by averaging the ΔF/F responses that gave a limited circular response (aka a light response with no triggered wave). A MATLAB code was then written to identify calcium transients that occur immediately following the light (within 2 seconds) and outside the boundary of the light response. The success chance of starting a wave was then computed by dividing the number of waves generated by the total number of stimuli (4–6) presented within a trial. Difference between groups was determined by performing a Kruskal-Wallis test followed by a Dunn-Šidák post-hoc correction.

The moment speed and area of wave propagation was determined for a subset of spontaneous and light-triggered waves (200 waves per group). To measure the mean moment speed of a wave, we used a Euclidean distance transform to measure the distances between the leading edge of the wave between pairs of frames. The mean distance travelled by the leading edge was divided by the time between frames to get a moment speed. The area of the wave was calculated by measuring the area of a maximum intensity projection of the binarized dF/dt stack (see above). The full code can be found at: https://github.com/Llamero/Retinal_Wave_Vector_Flow-Macro. Data are plotted using notched box plots with 95% CIs using the boxplot function in MATLAB.

To determine if RGCs participate similarly in spontaneous and light-triggered waves, we first calculated the peak ΔF/F of each neuron in the ganglion cell layer (GCL, 164 cells) during individual spontaneous and light-triggered waves (41 waves for each condition). Next, we generated a sorted cumulative distribution function (CDF), lowest to highest peak ΔF/F values, for each GCL neuron across spontaneous waves and light-triggered waves. We measured the distance between cumulative distributions using the D-statistic from the Kolmogorov-Smirnov (KS) test and the resulting distance matrix was used to cluster the RGCs using UPGMA hierarchical clustering. Statistical significance of the sorted samples from the dendrogram was then determined using 95% CI in a notch box plot.

To validate the above test and to exclude the possibility of the orientation of dendrogram branches contributing to a random sorting, we then measured the KS D-statistic between a linear CDF function (the extreme of a cell having the same peak ΔF/F in all waves) and measured CDFs for each RGC. These D-statistics were then sorted from smallest (a cell with the same peak ΔF/F in most waves) to largest (a cell reaching its peak ΔF/F in only a few waves). Statistical significance of the sorted samples from the D-statistic was then determined using 95% CI in a notch box plot.

To better visualize whether spontaneous and light-triggered waves recruit the same cells, we first grouped the cells in the ganglion cell layer based on the responses to the light flash as ON, OFF, ON-OFF, or NR cells. To do so, we calculated the mean ΔF/F for each cell one second after the light turned on and one second after the light turned off. Using a 15% ΔF/F threshold, we classified cells that responded only to the onset of the light as ON cells, cells that responded only to the offset of the light as OFF cells, cells that responded to both the onset and offset of the light as ON-OFF cells, and cells that did not respond at all as NR cells. This categorization is likely to overestimate the number of ON-OFF cells since at this age, cessation of ON responses in ON RGCs lead to a disinhibition of OFF RGCs (Akrouh and Kerschensteiner, 2013), which would appear to be an ON response given the temporal resolution of our imaging method. Importantly, this potential mis-classification does not impact the results since we are comparing the same cells in spontaneous and light evoked waves. Using this grouping, we then generated a heatmap of maximum ΔF/F of each cell during each individual spontaneous and light-triggered wave (columns in Figure 2c). The heatmaps were then clustered based on a chi-squared distance matrix using UPGMA hierarchical clustering.

Threshold-independent analysis of eye-specific segregation.—For every injection, we check the spatial extent of our fills by visualizing injected retinas. Only brains correspond to retinas with uniform labeling are cleared. Further, we confirm that the retina's projections to the superior colliculus are uniform. Brains with non-uniform labeling in retina or superior colliculus are discarded.

We first created masks that corresponded to the whole dLGN, vLGN, and OPN. To do so, the ipsi and contralateral channels were merged into a grayscale stack of images and the outline of each brain area was traced using a semi-automatic macro in imageJ. Axon bundles on the edges of the LGN were excluded from the brain tracings.

We applied an established threshold-independent protocol to investigate eye-specific segregation to three-dimensional brain structures [18]. To do so, every voxel within volumetric stacks obtained with light-sheet images were first made isotropic by binning the x and y dimension to match the resolution of the z-dimension (6.5 μm). Isotropic resolution was then verified by taking the FFT of several X-Z and X-Y projections. To determine background fluorescence, we obtained the mean fluorescence of the Alexa 488 and 647 dyes in non-retina-recipient targets and subtracted this background fluorescence from the raw stacks. We normalized fluorescence for each dye and each brain area by adjusting the contrast to 5% saturation.

For each voxel in each brain area, we computed the logarithm of the intensity ratio, $R = \log_{10}(F_i/F_c)$, where F_i is the fluorescence intensity in the ipsilateral channel and F_c is the fluorescence intensity in the contralateral channel of the corresponding voxel. We then computed the distribution of the values of R for all voxels in a single brain region or within quartiles of a brain region.

To compare R-distributions across animals, each distribution was shifted along the X-axis to align the maximal peak. This shift corrected for variations in values of R across images unrelated to segregation, such as the effectiveness of dye uptake and transport in axons, number of terminals/pixel, exposure times used in acquisition of the images, or other parameters that affect the absolute value of the intensities in each image. The distributions were also normalized so that the sum of values equaled 1.

To quantify differences between distributions, we calculated the variance and skew of the distributions. Variance is a measure of the spread of the distribution, which decreases if there is more overlap between ipsi and contralateral projections. The skew of the distribution also decreases if the contra-dominant peak is slightly shifted due to increased overlap in ipsi and contralateral labeling. Difference between groups was determined by performing an ANOVA followed by a Tukey-Kramer post-hoc test to account for unequal sample sizes.

Supplementary Material

Refer to Web version on PubMed Central for supplementary material.

Acknowledgements

We thank Eva K. Nichols and Professor Kaoru Saijo for help with implementation of CUBIC, the Berkeley Molecular Imaging Center for use of the Zeiss Lightsheet microscope and image analysis software, and members of the Feller Lab for commenting on the manuscript. A.T. and M.B.F. were supported by NIH ROI1EY019498 and RO1EY013528, and B.E.S. was supported by NIH P30EY003176.

References

Ackman JB, Burbridge TJ, and Crair MC (2012). Retinal waves coordinate patterned activity throughout the developing visual system. Nature 490, 219–225. [PubMed: 23060192]

Akerman CJ, Smyth D, and Thompson ID (2002). Visual experience before eye-opening and the development of the retinogeniculate pathway. Neuron 36, 869–879. [PubMed: 12467590]

Akerman CJ, Grubb MS, and Thompson ID (2004). Spatial and temporal properties of visual responses in the thalamus of the developing ferret. J. Neurosci 24, 170–182. [PubMed: 14715950]

Akrouh A, and Kerschensteiner D (2013). Intersecting circuits generate precisely patterned retinal waves. Neuron 79, 322–334. [PubMed: 23830830]

Arroyo DA, Kirkby LA, and Feller MB (2016). Retinal waves modulate an intraretinal circuit of intrinsically photosensitive retinal ganglion cells. J. Neurosci 36, 6892–6905. [PubMed: 27358448]

Assali A, Gaspar P, and Rebsam A (2014). Activity dependent mechanisms of visual map formation - From retinal waves to molecular regulators. Semin. Cell Dev. Biol 35, 136–146. [PubMed: 25152335]

Bialas AR, and Stevens B (2013). TGF-β signaling regulates neuronal C1q expression and developmental synaptic refinement. Nat. Neurosci 16, 1773–1782. [PubMed: 24162655]

Blankenship AG, and Feller MB (2010). Mechanisms underlying spontaneous patterned activity in developing neural circuits. Nat. Rev. Neurosci 11, 18–29. [PubMed: 19953103]

Blankenship AG, Ford KJ, Johnson J, Seal RP, Edwards RH, Copenhagen DR, and Feller MB (2009). Synaptic and extrasynaptic factors governing glutamatergic retinal waves. Neuron 62, 230–241. [PubMed: 19409268]

Blankenship AG, Hamby AM, Firl A, Vyas S, Maxeiner S, Willecke K, and Feller MB (2011). The role of neuronal connexins 36 and 45 in shaping spontaneous firing patterns in the developing retina. J. Neurosci 31, 9998–10008. [PubMed: 21734291]

Borghuis BG, Tian L, Xu Y, Nikonov SS, Vardi N, Zemelman BV, and Looger LL (2011). Imaging Light Responses of Targeted Neuron Populations in the Rodent Retina. J. Neurosci 31, 2855–2867. [PubMed: 21414907]

Borghuis BG, Looger LL, Tomita S, and Demb JB (2014). Kainate receptors mediate signaling in both transient and sustained OFF bipolar cell pathways in mouse retina. J. Neurosci 34, 6128–6139. [PubMed: 24790183]

Chen M, Weng S, Deng Q, Xu Z, and He S (2009). Physiological properties of direction-selective ganglion cells in early postnatal and adult mouse retina. J. Physiol 587, 819–828. [PubMed: 19103682]

Chew KS, Renna JM, McNeill DS, Fernandez DC, Keenan WT, Thomsen MB, Ecker JL, Loevinsohn GS, VanDunk C, Vicarel DC, et al. (2017). A subset of ipRGCs regulates both maturation of the circadian clock and segregation of retinogeniculate projections in mice. Elife 6.

Demas J, Sagdullaev BT, Green E, Jaubert-Miazza L, McCall MA, Gregg RG, Wong ROL, and Guido W (2006). Failure to Maintain Eye-Specific Segregation in nob, a Mutant with Abnormally Patterned Retinal Activity. Neuron 50, 247–259. [PubMed: 16630836]

Dhande OS, Hua EW, Guh E, Yeh J, Bhatt S, Zhang Y, Ruthazer ES, Feller MB, and Crair MC (2011). Development of single retinofugal axon arbors in normal and β2 knock-out mice. J. Neurosci 31, 3384–3399. [PubMed: 21368050]

Duncan MJ, Banister MJ, and Reppert SM (1986). Developmental appearance of light-dark entrainment in the rat. Brain Res 369, 326–330. [PubMed: 3697748]

Dunn FA, Della Santina L, Parker ED, and Wong ROL (2013). Sensory experience shapes the development of the visual system's first synapse. Neuron 80, 1159–1166. [PubMed: 24314727]

Ford KJ, Félix AL, and Feller MB (2012). Cellular mechanisms underlying spatiotemporal features of cholinergic retinal waves. J. Neurosci 32, 850–863. [PubMed: 22262883]

Hamby AM, Rosa JM, Hsu CH, and Feller MB (2015). CaV3.2 KO mice have altered retinal waves but normal direction selectivity. Vis. Neurosci 32, E003. [PubMed: 25873107]

Hong YK, Burr EF, Sanes JR, and Chen C (2018). Heterogeneity of retinogeniculate axon arbors. Eur. J. Neurosci

Hooks BM, and Chen C (2006). Distinct Roles for Spontaneous and Visual Activity in Remodeling of the Retinogeniculate Synapse. Neuron 52, 281–291. [PubMed: 17046691]

Huberman AD, Feller MB, and Chapman B (2008). Mechanisms underlying development of visual maps and receptive fields. Annu. Rev. Neurosci 31, 479–509. [PubMed: 18558864]

Jaepel J, Hübener M, Bonhoeffer T, and Rose T (2017). Lateral geniculate neurons projecting to primary visual cortex show ocular dominance plasticity in adult mice. Nat. Neurosci 20, 1708–1714. [PubMed: 29184207]

Johnson J, Wu V, Donovan M, Majumdar S, Rentería RC, Porco T, Van Gelder RN, and Copenhagen DR (2010). Melanopsin-dependent light avoidance in neonatal mice. Proc. Natl. Acad. Sci. U. S. A 107, 17374–17378. [PubMed: 20855606]

Kerschensteiner D (2016). Glutamatergic Retinal Waves. Front. Neural Circuits 10, 38. [PubMed: 27242446]

Kirkby LA, and Feller MB (2013). Intrinsically photosensitive ganglion cells contribute to plasticity in retinal wave circuits. Proc. Natl. Acad. Sci. U. S. A 110, 12090–12095. [PubMed: 23821744]

Kirkby LA, Sack GS, Firl A, and Feller MB (2013). A role for correlated spontaneous activity in the assembly of neural circuits. Neuron 80, 1129–1144. [PubMed: 24314725]

Liang L, Fratzl A, Goldey G, Ramesh RN, Sugden AU, Morgan JL, Chen C, and Andermann ML (2018). A Fine-Scale Functional Logic to Convergence from Retina to Thalamus. Cell 173, 1343–1355.e24. [PubMed: 29856953]

Morgan JL, Berger DR, Wetzel AW, and Lichtman JW (2016). The Fuzzy Logic of Network Connectivity in Mouse Visual Thalamus. Cell 165, 192–206. [PubMed: 27015312]

Murata Y, and Colonnese MT (2016). An excitatory cortical feedback loop gates retinal wave transmission in rodent thalamus. Elife 5, 1–19.

Puthussery T, Percival KA, Venkataramani S, Gayet-Primo J, Grünert U, and Taylor WR (2014). Kainate receptors mediate synaptic input to transient and sustained OFF visual pathways in primate retina. J. Neurosci 34, 7611–7621. [PubMed: 24872565]

Rao S, Chun C, Fan J, Kofron JM, Yang MB, Hegde RS, Ferrara N, Copenhagen DR, and Lang RA (2013). A direct and melanopsin-dependent fetal light response regulates mouse eye development. Nature 494, 243–246. [PubMed: 23334418]

Renna JM, Weng S, and Berson DM (2011). Light acts through melanopsin to alter retinal waves and segregation of retinogeniculate afferents. Nat. Neurosci 14, 827–829. [PubMed: 21642974]

Rompani SB, Müllner FE, Wanner A, Zhang C , Roth CN, Yonehara K, and Roska B (2017). Different Modes of Visual Integration in the Lateral Geniculate Nucleus Revealed by Single-Cell-Initiated Transsynaptic Tracing. Neuron 93, 767–776.e6. [PubMed: 28231464]

Rosa JM, Morrie RD, Baertsch HC, and Feller MB (2016). Contributions of rod and cone pathways to retinal direction selectivity through development. J. Neurosci 36, 9683–9695. [PubMed: 27629718]

Slaughter MM, and Miller RF (1981). 2-amino-4-phosphonobutyric acid: a new pharmacological tool for retina research. Science 211, 182–185. [PubMed: 6255566]

Sommeijer J-P, Ahmadlou M, Saiepour MH, Seignette K, Min R, Heimel JA, and Levelt CN (2017). Thalamic inhibition regulates critical-period plasticity in visual cortex and thalamus. Nat. Neurosci 20, 1715–1721. [PubMed: 29184199]

Soto F, Ma X, Cecil JL, Vo BQ, Culican SM, and Kerschensteiner D (2012). Spontaneous Activity Promotes Synapse Formation in a Cell-Type-Dependent Manner in the Developing Retina. J. Neurosci 32, 5426–5439. [PubMed: 22514306]

Thompson A, Gribizis A, Chen C, and Crair MC (2017). Activity-dependent development of visual receptive fields. Curr. Opin. Neurobiol 42, 136–143. [PubMed: 28088066]

Tian N, and Copenhagen DR (2003). Visual Stimulation Is Required for Refinement of ON and OFF Pathways in Postnatal Retina Ning. Neuron 39, 85–96. [PubMed: 12848934]

Torborg CL, and Feller MB (2004). Unbiased analysis of bulk axonal segregation patterns. J. Neurosci. Methods 135, 17–26. [PubMed: 15020085]

Xu H, Chen H, Ding Q, Xie Z-H, Chen L, Diao L, Wang P, Gan L, Crair MC, and Tian N (2010). The Immune Protein CD3ζ Is Required for Normal Development of Neural Circuits in the Retina. Neuron 65, 503–515. [PubMed: 20188655]

Zariwala HA, Borghuis BG, Hoogland TM, Madisen L, Tian L, De Zeeuw CI, Zeng H, Looger LL, Svoboda K, and Chen T-W (2012). A Cre-Dependent GCaMP3 Reporter Mouse for Neuronal Imaging In Vivo. J. Neurosci 32, 3131–3141. [PubMed: 22378886]

Zheng J, Lee S, and Zhou ZJ (2006). A transient network of intrinsically bursting starburst cells underlies the generation of retinal waves. Nat. Neurosci 9, 363–371. [PubMed: 16462736]

Highlights:

- Glutamatergic retinal waves are triggered by spots of light.
- Triggered waves are mediated by rods and cones.
- Triggered waves and spontaneous waves have the same spatiotemporal properties.
- Dark-rearing prior to eye-opening reduces segregation of retinogeniculate axons.

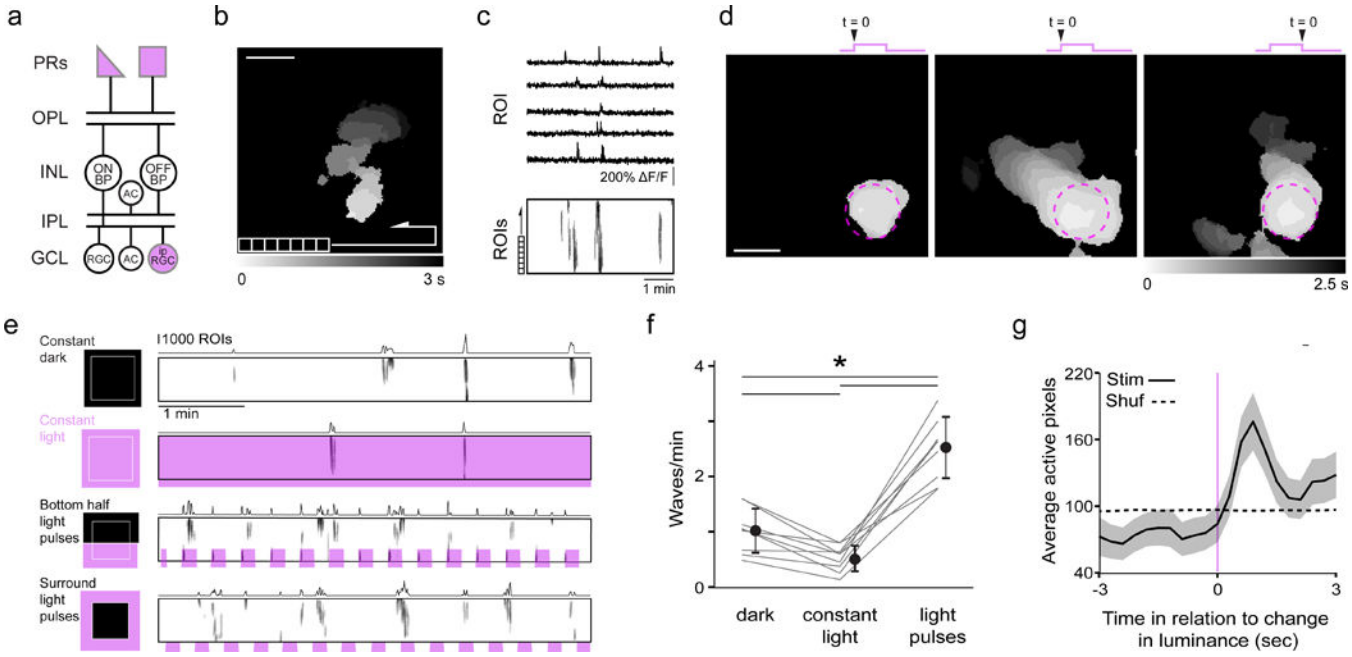

Figure 1. Light modulates the frequency of glutamatergic waves.

a. Schematic of retinal circuitry in P10–14 mice when glutamatergic waves occur. Purple indicates light-sensitive cells. OPL: outer plexiform layer; INL: inner nuclear layer; IPL: inner plexiform layer; GCL: ganglion cell layer; RGC: retinal ganglion cell; ipRGC: intrinsically photosensitive RGC; AC: amacrine cell.

b. Heat map representing the spread of a representative glutamatergic wave observed with two-photon calcium imaging in retina expressing GCaMP6f in synapsin-1 positive cells. For subsequent analysis, *th*e field of view (FOV; 850 μm x 850 μm) is divided into a grid of 10,000 regions of interests (ROI). Scale bar = 200 μm.

c. (Top) Time course of the fractional change in fluorescence (ΔF/F) for five example ROIs acquired at a frame rate of 3 Hz. (Bottom). Raster plots of neuronal Ca^{2+} transients > 15% ΔF/F for all ROIs. The total imaging duration is 5 minutes.

d. Examples of light stimulation of P12 retinas using a 200 μm diameter spot of 375 nm light within the FOV. The stimulation evoked light responses for neurons within the illuminated spot (purple dashed circle) but sometimes did not trigger a wave (left), or triggered a wave on the onset (middle) or the offset (right) of a light response.

e. Raster plots depicting retinal waves under four conditions: dark, constant light, light pulses across the bottom of the FOV, and light pulses surrounding the FOV. The sum of active ROIs is displayed above each raster plot. See Supplementary Movie 1. For subsequent analyses, the two light-pulse conditions were combined.

f. Summary data depicting mean ± SD wave frequency for dark, light, and pulsing light conditions. *: $p < 0.001$ Tukey's HSD test, n = 9 retinas per group.

g. Waveform average depicting sum of ROIs ± SEM triggered around changes in luminance at P11–13 (black). Dotted line represents the same dataset randomly shuffled in time.

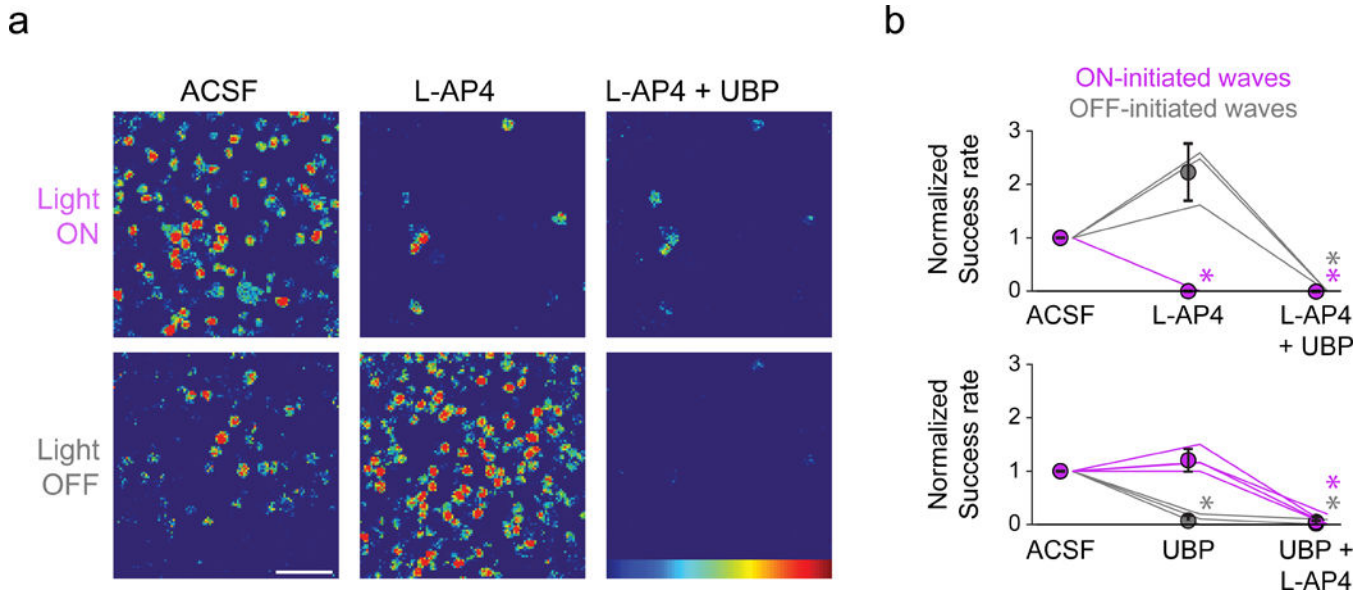

Figure 2. Blocking photoreceptor to bipolar cell signaling abolishes light-evoked wave initiation.

a. Heatmaps representing ΔF/F of example RGC responses to light onset and offset in ACSF (left), L-AP4 (middle), and L-AP4+UBP 310 (right). Note ipRGC responses are preserved during light onset in presence of photoreceptor-bipolar cell antagonists (top right). Scale bar = 50 μm.

b. Light modulates the frequency of glutamatergic waves via activation of conventional photoreceptors. Top: Summary data depicting mean success rate of starting a wave on either the onset or offset of a light stimulus. n = 3 retinas per group. Bottom: Same as top but the order of the drugs was switched. n = 4 retinas per group. Error bars, SD. *p < 0.05 Dunn-Sidak.

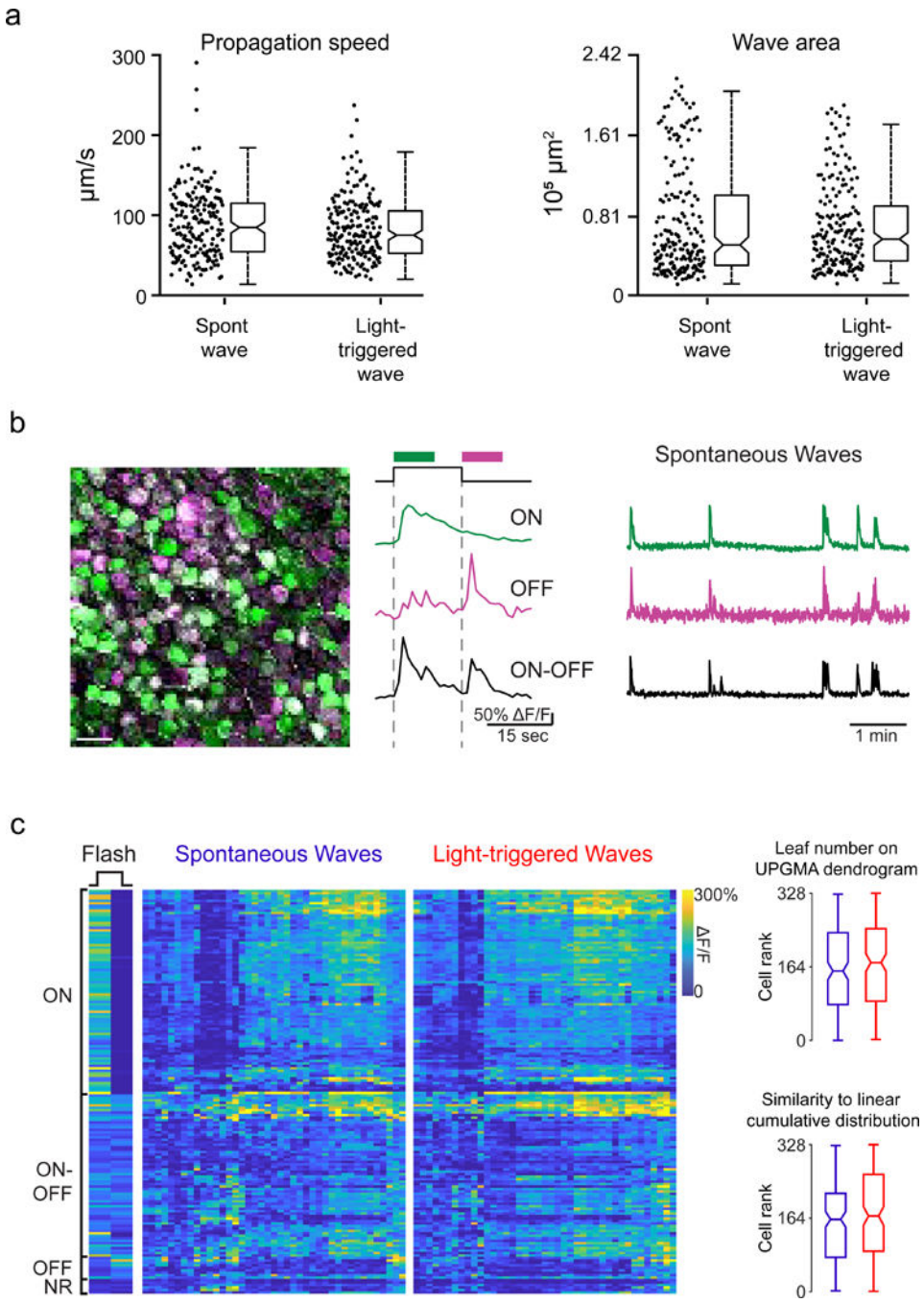

Figure 3. Light-triggered and spontaneous waves have similar spatiotemporal properties and recruit the same retinal circuits.

a. Summary data depicting wave propagation speed and wave propagation area for spontaneous and light-evoked waves. Notches: 95% CI.

b. Left: Pseudocolored representation of 164 RGCs responding to light onset (ON; green), light offset (OFF; magenta) or both (ON-OFF; white). Colored traces are example ΔF/F responses of individual RGCs to the flash of light. Right: example traces of spontaneous activity over 5 minutes for the same cells. Scale bar = 30 μm.

c. Left: RGCs were characterized by their light response (NR = no light response). Middle: Heatmap depicting max intensity of an RGC ΔF/F response (row) during each spontaneous and light-triggered wave (column). The rows are ordered based on light response. The columns are ordered based on similarity between waves. Right: Notched box plot representing leaf number distributions (top) or rank (bottom) of RGCs as they participate in spontaneous (blue) and light-triggered (red) waves. The leaf numbers come from a dendrogram that was generated using UPGMA hierarchical clustering of RGC activity profiles during spontaneous and light-triggered waves. Notches represent 95% CI. Rank is based on similarity to a model cell that responded equally to every wave. 0 is most similar.

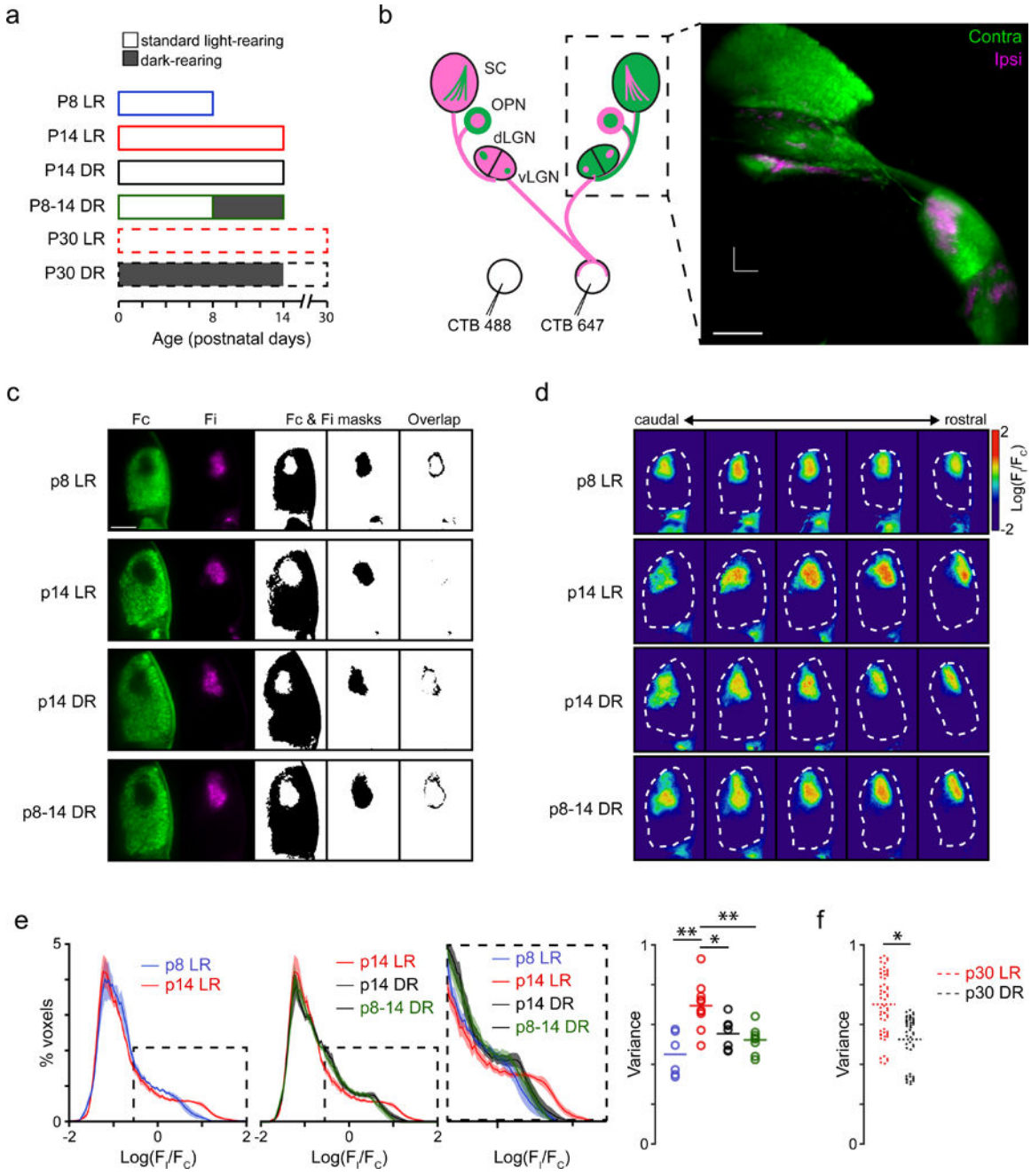

Figure 4. Mice reared in darkness before eye-opening exhibit reduced eye-specific segregation.

a. Schematic of experimental groups used in this study. LR: 12-hour day/night cycle; DR: dark-reared, 24-hour night cycle.

b. Left: Schematic representation of the experiment performed to investigate eye-specific segregation of retinal projections to multiple brain regions. Intraocular injection of anterograde tracers cholera toxin subunit B conjugated to Alexa 488 or Alexa 647 were used to visualize the retinal projections to the dorsal and ventral lateral geniculate nucleus (dLGN, vLGN), the olivary pretectal nucleus (OPN), and the superior colliculus (SC). Right: max intensity projection image of three-dimensional reconstruction of retinal projections to

the vLGN, dLGN, OPN, and SC obtained by light-sheet imaging of cleared brains. Scale bar = 500 μm. See Supplementary Movies 2 and 3).

c. Optical coronal slices of the dLGN in P8 LR, P14 LR, P14 DR, and P8-P14 DR mice. First two columns are fluorescence images of retinal projections from the contralateral (green) and ipsilateral (magenta) eye. For display purposes, fluorescence is masked using a threshold (Fc and Fi masks; middle columns) and the overlap between the two is calculated (right).

d. Optical coronal slices depicting the log-ratio [log R = $\log_{10}$(Fi/Fc)] of ipsi-to-contralateral fluorescence across the anterior third section of the dLGN. Examples from the same brains as panel c.

e. Eye-specific segregation was represented by the distribution of the log-ratio (log R) of ipsi-to-contra fluorescence for all voxels within the dLGN. The positive values in the distribution represent voxels with greater ipsilateral fluorescence (e.g., see inset: increased segregation indicated by broader distribution). The variance of the distributions was used to compare across conditions (e.g. dotted lines indicate how less segregation would alter the distributions). Right: Summary data comparing variance of log R distributions across P8 LR, P14 LR, P14 DR, and P8-14 DR conditions. $F(3,27) = 9.28$, $p = 0.0002$; **: $p < 0.01$; *: $p < 0.05$ ANOVA followed by Tukey-Kramer post-hoc test.

f. Summary data comparing variance of log R distributions between p30 LR and p30 DR (dark-reared P0–14 and subsequently light-reared P15-P30). *: $p < 0.05$ unpaired t-test.